Journal of Contaminant Hydrology 142–143 (2012) 33–49

Contents lists available at SciVerse ScienceDirect

Journal of Contaminant Hydrology

journal homepage: www.elsevier.com/locate/jconhyd

Long-term electrical resistivity monitoring of recharge-induced contaminant plume behavior

Erika Gasperikova [a,*], Susan S. Hubbard [a], David B. Watson [c], Gregory S. Baker [b], John E. Peterson [a], Michael B. Kowalsky [a], Meagan Smith [b], Scott Brooks [c]

[a] Lawrence Berkeley National Laboratory, 1 Cyclotron Road, MS 74R0120, Berkeley, CA 94720, United States
[b] University of Tennessee, Department of Earth and Planetary Sciences, 1412 Circle Drive, Knoxville, TN 37996, United States
[c] Oak Ridge National Laboratory, 1 Bethel Valley Road, MS 6038, Oak Ridge, TN 37831-6038, United States

ARTICLE INFO

Article history:
Received 1 March 2012
Received in revised form 25 September 2012
Accepted 26 September 2012
Available online 4 October 2012

Keywords:
Electrical resistivity
Contaminant plume
Time-lapse monitoring
Nitrate
Rainfall

ABSTRACT

Geophysical measurements, and electrical resistivity tomography (ERT) data in particular, are sensitive to properties that are related (directly or indirectly) to hydrological processes. The challenge is in extracting information from geophysical data at a relevant scale that can be used to gain insight about subsurface behavior and to parameterize or validate flow and transport models. Here, we consider the use of ERT data for examining the impact of recharge on subsurface contamination at the S-3 ponds of the Oak Ridge Integrated Field Research Challenge (IFRC) site in Tennessee. A large dataset of time-lapse cross-well and surface ERT data, collected at the site over a period of 12 months, is used to study time variations in resistivity due to changes in total dissolved solids (primarily nitrate). The electrical resistivity distributions recovered from cross-well and surface ERT data agrees well, and both of these datasets can be used to interpret spatiotemporal variations in subsurface nitrate concentrations due to rainfall, although the sensitivity of the electrical resistivity response to dilution varies with nitrate concentration. Using the time-lapse surface ERT data interpreted in terms of nitrate concentrations, we find that the subsurface nitrate concentration at this site varies as a function of spatial position, episodic heavy rainstorms (versus seasonal and annual fluctuations), and antecedent rainfall history. These results suggest that the surface ERT monitoring approach is potentially useful for examining subsurface plume responses to recharge over field-relevant scales.

Published by Elsevier B.V.

1. Introduction and background

The DOE Oak Ridge Integrated Field Research Challenge (IFRC) site, near Oak Ridge, Tennessee, was established to investigate long-term immobilization strategies and to improve the understanding of rates and mechanisms that control contaminant fate and transport from the plot scale to the watershed scale. The nearby Oak Ridge National Laboratory was established in 1943 as part of the wartime effort, with an immediate goal of separating and producing uranium and plutonium for use in developing a nuclear weapon. In 1951, four unlined impoundments were constructed at the Y-12 Plant in Bear Creek Valley, TN. These impoundments, which are known as the S-3 ponds, received liquid wastes generated from uranium operations at the Y-12 Plant, primarily acidic uranium nitrate but with contributions from other processes, as well as liquid wastes and sludges from other sites (U.S. DOE, 1997). The composition of the sludges and liquids in the ponds varied from pond to pond and temporally (Brooks, 2001). However, the liquid waste in the ponds can be generally described as highly acidic (primarily nitric acid). In 1983 waste discharges to the ponds ceased, and the remaining pond waste was treated by in situ neutralization and biodenitrification. After this treatment, the sludges were allowed to settle and the

* Corresponding author. Tel.: +1 510 486 4930; fax: +1 510 486 5686.
E-mail addresses: egasperikova@lbl.gov (E. Gasperikova), sshubbard@lbl.gov (S.S. Hubbard), watsondb@ornl.gov (D.B. Watson), gbaker@tennessee.edu (G.S. Baker), jepeterson@lbl.gov (J.E. Peterson), mbkowalsky@lbl.gov (M.B. Kowalsky), msmith79@utk.edu (M. Smith), brookssc@ornl.gov (S. Brooks).

0169-7722/$ – see front matter. Published by Elsevier B.V.
http://dx.doi.org/10.1016/j.jconhyd.2012.09.007

supernatant liquid pumped off and treated for removal of organic contaminants and metals. Although the area was capped and now serves as a parking lot, the contaminants have infiltrated into the groundwater of the highly structured saprolitic subsurface, resulting in a variety of plumes that now extend almost five kilometers downgradient from the basin location. A key hypothesis for the IFRC study is that recharge is the main hydraulic driver for groundwater flow and dilution of contaminants along flow pathways, as it dictates the temporal and spatial variability of geochemical and microbiological processes.

Our objective is to examine the impact of freshwater recharge on contaminant dilution and mobility, and particularly, to explore the use of geophysical methods for assessing associated subsurface hydrogeochemical processes that are often difficult to ascertain using wellbore data alone. We explore the utility of time-lapse electrical resistivity tomography (ERT) for quantifying the spatiotemporal distribution of nitrate concentration as a function of recharge, scale, and subsurface heterogeneity.

Subsurface electrical properties depend on the solid and fluid constituents and on their spatial and temporal variations. Due to the sensitivity of electrical resistivity (or its inverse electrical conductivity) to environmental variables, such as fluid saturation or contaminant concentration, ERT is often used for monitoring using a time-lapse approach. With this approach, electrical measurements are repeated at the same locations during a dynamic event, highlighting temporal changes in geophysical properties and removing the effects of geological heterogeneity. The use of ERT for monitoring environmental variables has been demonstrated in many investigations. Examples include the monitoring of leakage from underground tanks (Daily et al., 2004a, 2004b; Ramirez et al., 1996), leakage through hydrological barriers (Daily and Ramirez, 2000), remediation treatments and responses (Commer et al., 2011; Daily and Ramirez, 1995; Ramirez et al., 1993; Slater and Binley, 2003), the movement of water or dissolved solutes in the subsurface (Binley et al., 2002; Chambers et al., 2004; Daily et al., 1992; French et al., 2002; Kemna et al., 2002; Koch et al., 2009; Miller et al., 2008; Oldenborger et al., 2007; Park, 1998; Singha and Gorelick, 2005; Slater et al., 2002; Zhou et al., 2001) and hyporheic zone processes (Ward et al., 2010).

Several recent studies that involve ERT have been performed at the Oak Ridge IFRC study site. Watson et al. (2005) collected ERT and seismic tomography data next to the contaminant basins and used them to delineate regions of high-ionic strength associated with the contaminant plume, and to identify the transition zone between shallower saprolite and a deeper bedrock unit. Groundwater nitrate concentrations from three wells in the study area agreed well with their electrical resistivity interpretation, indicating relatively lower resistivity values in the areas with high nitrate concentrations and higher resistivity values in the areas with lower nitrate concentrations. Kowalsky et al. (2011) used a coupled hydrological and ERT modeling approach to incorporate various time-lapse datasets (hydrogeological, geochemical, and geophysical) at the local scale and to exploit those data to estimate permeability, porosity, and various petrophysical parameters. They applied this approach to cross-well ERT and wellbore hydrological measurements, collected over the course of a month near the seepage basins, to estimate hydrological and geophysical properties of various subsurface units, and to explore short-term, local-scale recharge phenomena.

We build upon these previous studies to explore how the electrical response varies due to changes in recharge and associated contaminant dilution over plume scales and annual timeframes. We also examine the overall benefits and limitations of using ERT for monitoring plume-scale behavior. For this study, we use time-lapse surface and cross-well ERT data and associated wellbore geochemical data that have been co-collected over a 12-month timeframe, which includes a dry period, a wetting-up period, and a wet period. From a process perspective, our challenge is to determine if the time-lapse ERT data can be useful for quantifying spatiotemporal variations in recharge-related plume behavior, which can then be used to inform reactive transport modeling ongoing at the site (Tang et al., 2010). From a geophysical perspective, our challenge is to determine the sensitivity of the electrical response to changes in nitrate concentrations in the saturated zone with the additional complication of strongly dipping geological heterogeneity.

After brief descriptions of the electrical resistivity method, inversion technique, and petrophysical models used in our study (Section 2), we describe the site geology and hydrogeochemistry (Section 3), and the acquired time-lapse geophysical and geochemical data sets (Section 4). We then illustrate how the small- and large-scale measurements can be assessed to provide insights about recharge-based plume behavior at the contaminated IFRC study site (Sections 5–7).

2. Electrical resistivity method

Electrical resistivity (the reciprocal of electrical conductivity) is the property of a material representing its resistance to a current flow. The resistivity is defined by Ohm's law:

$$\mathbf{E} = \rho \mathbf{J} \text{ or } \mathbf{J} = \sigma \mathbf{E}, \tag{1}$$

where $\mathbf{E}$ is the electric field in volts per meter (V/m), $\mathbf{J}$ is the current density in amperes per square meter (A/m^2), ρ is the resistivity in Ohm-meters (Ω-m) and σ is the electrical conductivity in siemens per meter (S/m) (reciprocal of electrical resistivity, $\sigma = 1/\rho$). Electrical conductivity is a measure of a material's ability to conduct an electric current.

Electrical resistivity methods use an array of four electrodes to measure the subsurface resistivity; a known current is injected between two electrodes, and the potential difference is measured across the other two electrodes. The measured electrical potential is used together with the injected current and a geometric factor that is a function of these four electrode distances, to calculate an apparent resistivity for uniform subsurface conditions following Ohm's law. When the ground is uniform, the apparent resistivity is constant and independent of both electrode location and surface location. When subsurface inhomogeneities are present, the apparent resistivity varies with the relative electrode positions. It is important to note that surface resistivity measurements encompass the integrated effect of the subsurface resistivity structure to the depth of current penetration. In homogeneous ground the depth of current penetration increases as the separation distance between current electrodes increases. When the

distance between current electrodes is twice that of a given depth, half of the current flows above and half below this depth (Telford et al., 1990). The volume of the ground close to the array dictates the mean value of the apparent resistivity. As the array expands, larger and larger volumes of the ground are included. The aim of the interpretation is to determine the changes in actual ground resistivity that cause the changes in the measured apparent resistivity by matching the observed apparent resistivity values to numerically simulated values for two-dimensional (2D) or three-dimensional (3D) models as described below.

Resistivity data inversion is a nonlinear iterative process. For a nonlinear inverse problem, the data vector **d** is a nonlinear function of the model parameter vector **m**, that is, $\mathbf{d}=g(\mathbf{m})$. The objective of smooth model inversion, also known as Occam's inversion (Constable et al., 1987), is to minimize a weighted data misfit,

$$\mathbf{S}(\mathbf{m}) = (\mathbf{d}_{obs}-g(\mathbf{m}))^T\mathbf{W}_d(\mathbf{d}_{obs}-g(\mathbf{m})) + \alpha\ \mathbf{m}^T\mathbf{R}\,\mathbf{m}, \tag{2}$$

where $\mathbf{d}_{obs}$ is the observed data, $g(\mathbf{m})$ is the calculated data, $\mathbf{W}_d$ is a data weighting matrix, α is a Lagrange multiplier and a stabilizing factor, and **R** is roughness operator. The nonlinear inverse problem is solved iteratively where, at a given iteration, the inverse problem is linearized around the model parameters of the previous iteration, and the sensitivities of the model parameters with respect to the data (i.e., the Jacobian or sensitivity matrix) are used to find an updated model with improved data fit. The smooth model inversion finds the smoothest possible model whose response fits the data to the a-priori Chi-squared statistic under the assumption of a Gaussian distribution of data errors. The goodness of fit is characterized by the root mean squared (RMS) error, in percent, given by

$$RMS = \sqrt{\frac{\sum_{i=1}^{N}\left(\frac{d_i^{pred}-d_i^{meas}}{d_i^{meas}}\right)^2}{N}} \times 100, \tag{3}$$

where N is the total number of data points, and d_i^{pred} and d_i^{meas} are the predicted and measured values, respectively, of data point i. Another measure of the goodness of fit is the L2-norm, defined as the sum of the squared weighted data errors:

$$L2-norm = \sum_{i=1}^{N}\left(\frac{d_i^{pred}-d_i^{meas}}{W_i}\right)^2 \tag{4a}$$

where W_i is the data weight, and d_i^{pred} and d_i^{meas} are the predicted and measured values, respectively, of data point i. Since the number of measurements varies from data set to data set, the normalized L2-norm is used:

$$\text{Normalized L2} - \text{norm} = \text{L2} - \text{norm/N}. \tag{4b}$$

When the normalized L2-norm is less than or equal to one, the inversion has converged to the solution.

In the time-lapse inversions, the background data are inverted using a standard inversion method to reconstruct the background (reference) resistivity model. The subsequent data sets are inverted using the algorithm of LaBrecque and Yang (2001), using apparent resistivity values, that inverts the difference between the monitoring and background data sets, and the reference resistivity model is used as the a-priori model.

In the near surface, the resistivity of geological materials is often expressed using Archie (1942) empirical law as a function of porosity, fluid saturation, and pore fluid resistivity as

$$\rho_b = a\ \phi^{-m}\ S_w^n\ \rho_f, \tag{5}$$

where ρ_b is the bulk resistivity of the media, a is the proportionality constant, ϕ is the porosity, m is the cementation factor, S_w is the water saturation, n is the saturation exponent (usually assumed to equal 2), and ρ_f is the resistivity of the pore fluid, which is sensitive to different environmental variables, as described below. The value of Archie's relationship for hydrological applications is that it links electrical measurements to groundwater quality and hydrological properties.

The resistivity of the pore fluid decreases with increasing temperature because the mobility of the ions in solution increases with temperature. While soil temperature variations are often small and thus negligible in the saturated zone, they usually have to be accounted for in ERT time-lapse interpretations of soil and vadose zones, as in some cases the effect of temperature variations on the electrical response is larger than the effect of variations in pore fluid chemistry or saturation (e.g., Hayley et al., 2007; Rein et al., 2004). An approximate formula for the pore fluid resistivity ρ_f as a function of temperature t is given by Keller and Frischknecht (1996):

$$\rho_f(t) = \frac{\rho_{18^\circ C}}{1+\alpha(t-18)}, \text{where } \alpha \cong 0.025. \tag{6}$$

The pore fluid resistivity (and thus bulk resistivity) is also dependent on salinity. Empirical relationships can be used to relate the electrical conductivity of aqueous solutions to the total-dissolved-solids (TDS) (Fishman and Friedman, 1989):

$$\sigma_w \cong b\ *\ TDS, \tag{7}$$

where, depending upon the ionic composition and temperature of the solution, the constant b can range from ~1.2×10^{-4} to ~2.0×10^{-4} with TDS given in mg/l. An average value of $b=1.5\times10^{-4}$ is typically used to predict the conductivity of natural waters at 25 °C (Fishman and Friedman, 1989). Site-specific relationships between fluid conductivity and TDS (or a particular contaminant concentration) are also commonly developed; this is especially so for sites with extreme or atypical geochemical conditions, such as at the Oak Ridge IFRC. This linear relationship shown in Eq. (7) suggests that an order of magnitude change in TDS will cause an order of magnitude change in fluid conductivity (and, through Eq. (5), in bulk resistivity) that could potentially be detected by ERT monitoring.

3. Study site hydrogeology and geochemistry

The study site is located to the west and downgradient of the former S-3 ponds (seepage basins) that were used to

dispose of contaminants, as discussed earlier. Historical disposal of liquid wastes within the ponds has resulted in extensive subsurface contamination in the vadose zone and the groundwater; several of the groundwater plumes now extend almost five kilometers downgradient from the site of the former ponds.

The study region is located within the Valley and Ridge physiographic province of the Appalachians, and contains complex dipping strata of upper Cambrian age (Hatcher et al., 1992). In some locations, the study site is underlain by ~2-m thick horizontal fill layer that was emplaced following excavation of contaminated soils. Below the fill are geological layers that dip ~45° to the southeast and have a strike of N55E (parallel to the Bear Creek Valley). These layers include (from shallower to deeper) unconsolidated saprolite (typically 3–10 m thick), a transition zone of weathered fractured bedrock (4–16 m thick), and a deeper more competent bedrock called the Nolichucky Shale, which is composed of interbedded shales and limestones (Fig. 1).

The water table is ~4–5 m below ground surface, depending on seasonal and recharge conditions. The site is located within a valley and adjacent to Bear Creek; several tributaries crosscut the plume. Groundwater flow is oriented predominantly along the geological strike, but can be influenced by local topography with discharge occurring at Bear Creek and its tributaries.

There are several potential pathways and mechanisms that influence flow and transport in the subsurface. The transition zone is moderately weathered and highly fractured. Since the hydraulic conductivity of the transition zone can be several orders of magnitude larger than the saprolite and bedrock zones, the transition zone serves as a preferential flowpath for groundwater and contaminants (Chen et al., 2006, 2010; Kowalsky et al., 2011; Solomon et al., 1992). Bedding planes and remnant fracturing in the saprolite also serve as flow pathways. Although fractures dominate flow and transport, diffusion of solutes between the fractures and the matrix is also a significant transport mechanism; the silt/clay rich matrix is conceptualized to serve as a persistent secondary source of groundwater contamination (Roden and Scheibe, 2005; Watson et al., 2005). The climate in the region can be categorized as humid continental. The average annual precipitation is 1.4 m as measured at the Oak Ridge ATDD Weather Station. Monthly average precipitation values range from ~0.076 m to ~0.15 m; precipitation tends to be greater in July due to thunderstorm activity, and lower in the fall months when high-pressure systems are frequent.

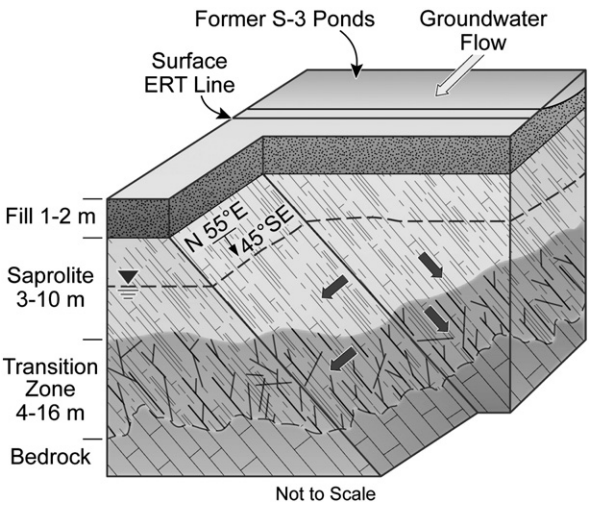

Fig. 1. Schematic of hydrogeological setting at the study site and approximate thickness of key units. The thick black arrows indicate conceptualized flow pathways along geologic strike and bedding planes.

Groundwater contaminants near the former disposal ponds include nitrate (up to 40,000 mg/l), sulfate (up to 3000 mg/l), uranium (up to 50 mg/l), technetium-99 (up to 40,000 pCi/l), and tetrachloroethylene (up to 9 mg/l) (USDOE, 1997; Wu et al., 2006). The groundwater near the seepage basins is very acidic, with pH ranging from 2.7 to 4.8. Due to dilution, expulsion of solutes from the matrix, and pH-dependent geochemical reactions, the groundwater aqueous geochemistry is expected to change upon contact with subneutral pH rainfall that has infiltrated through the vadose zone. Zhang et al. (2008) describe ion exchange, precipitation/dilution, and adsorption/desorption reactions expected for the site groundwater as a function of pH. Van der Hoven et al. (2005) used natural tracers at the site to document that geochemical conditions varied over space, time, and as a function of geological unit during storm and nonstorm events. Although Van der Hoven et al. (2005) identified the difficulty in using data from wellbores (which are typically screened over particular depth intervals only) to delineate trends, they hypothesized that the recharge-based oscillations of chemical conditions in the shallow groundwater are likely to have significant implications for solute transport. The complexity of the hydrogeology and geochemistry and their interactions over space and time render interpretations of groundwater plume response to recharge difficult using borehole data only (Kowalsky et al., 2011; Van der Hoven et al., 2005).

Although ongoing experimental and numerical studies are exploring more complex geochemical responses to rainfall in ORNL sediments and the associated geophysical response to those changes (Revil et al., in press), here we focus on exploring the use of time-lapse ERT to monitor and estimate only nitrate groundwater concentrations. Nitrate is a widespread groundwater contaminant, often stemming from leaking septic tanks and agricultural practices. At the Oak Ridge site, nitric acid was used for the extraction and processing of radioactive metals. The drinking-water standard of 10 mg/l nitrate as nitrogen has been established (U.S. Environmental Protection Agency, 2005). Although having nitrate concentrations at or below the maximum contaminant level (MCL) is not generally an adult public-health threat, nitrate in drinking water can cause low oxygen levels in the blood, which is a potentially fatal condition for infants (Spalding and Exner, 1993). Additionally, and important for this study, nitrate can serve as an oxidant to uranium, transforming immobile U(IV) to mobile U(VI) (Wu et al., 2010). With high concentrations of both nitrate and uranium at the S-3 ponds and with high average annual precipitation rates, it is critical to gain an understanding of how nitrate concentrations at the site vary with recharge.

4. Datasets

In this section we describe the acquisition, analysis and inversion of data used for this study, including the surface and cross-well ERT, EM induction wellbore measurements, precipitation, and wellbore geochemical datasets.

4.1. Surface ERT

Twenty-eight surface ERT datasets were collected along the same profile (Fig. 2) at various time intervals between the fall of 2008 and the fall of 2009 (Fig. 3) using an AGI SuperSting R8/IP system. The surface ERT line (red solid line in Fig. 2c and red dashed line in Fig. 2d) used for extensive time-lapse monitoring extends from southeast (SE) to northwest (NW). The profile spans the downgradient border of the S-3 ponds and runs perpendicular to both the direction of groundwater flow and geological strike. The 83 m long surface monitoring ERT profile had 112 permanently installed electrodes spaced 0.75 m apart. A combination of dipole–dipole, Wenner, and Schlumberger arrays was used for data acquisition. Each surface resistivity dataset contained about 11,600 measurements, which included repeat and reciprocal measurements that were included to help identify and remove noisy data. A typical acquisition time for each dataset was 8 h. This acquisition time could be significantly reduced after an optimal configuration that requires much fewer repeat and reciprocal measurements is established. During the March 2010 field campaign we verified that data acquired with an optimized four-hour acquisition schedule provided the same information as the data from an eight-hour acquisition. Measurements that differed by more than 3% from their repeat or reciprocal measurements were removed from the data set; the remaining pairs repeated for a given survey were averaged. In addition, data points with low current (<100 mA) and low voltage (<2 mV) were

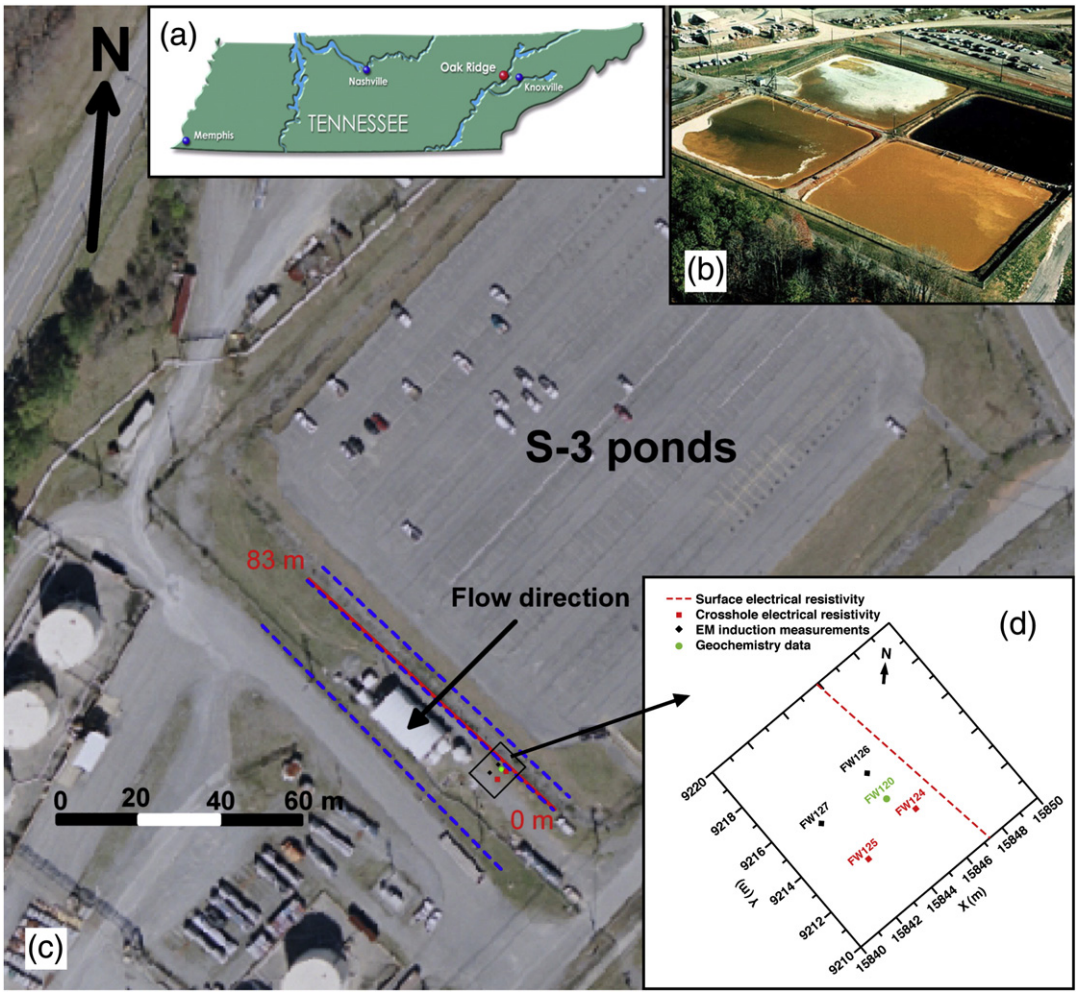

Fig. 2. Oak Ridge Integrated Field Research Challenge (IFRC) site: (a) location in eastern Tennessee, (b) unlined surface trenches (the S-3 Ponds) that received acidic nitrate and uranium waste from 1951 to 1983, (c) parking lot covering S-3 Ponds after they were capped in 1988 and location of surface and borehole ERT arrays (in red) downgradient from the parking lot. The flow direction is indicated by a long black arrow. Blue dashed lines indicate locations of additional surface ERT profiles shown in Fig. 7. (d) Detailed location map near ERT boreholes and FW120, where geochemical and EM induction data were collected.

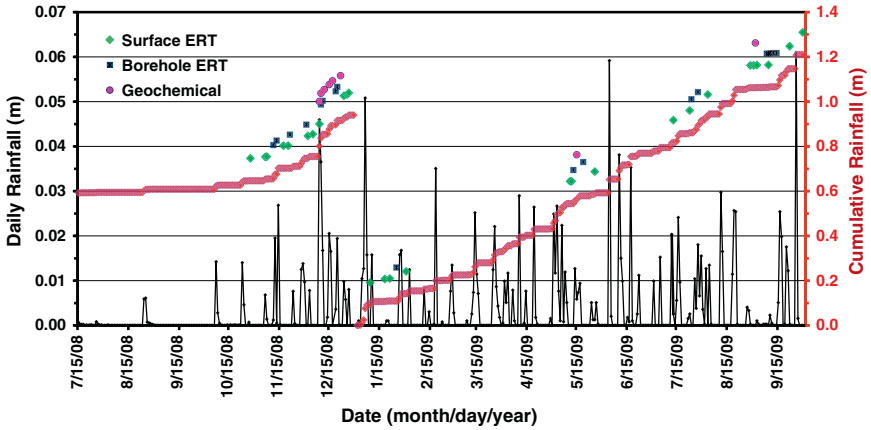

Fig. 3. Daily rainfall (m) in black, cumulative rainfall (m) in red, geochemical in magenta, surface ERT in green, and cross-well ERT data in blue plotted as a function of time from 07/2008 until 10/2009.

removed. Typically, less than 1% of the repeat and reciprocal measurements had an error larger than 3%, and less than 10% of the data were removed because of low measured signals.

In addition to this monitoring transect, we also collected three parallel profiles (blue dashed lines in Fig. 2c) during a single acquisition campaign (March 2010) to assess resistivity variations downgradient from the source and along geological strike.

4.2. Cross-well ERT

The cross-well ERT pair (red squares in Fig. 2c and d) forms a plane that is perpendicular to the surface line and aligned with the groundwater flow direction and geological strike. The boreholes used to acquire the cross-well data (FW124 and FW125) are 3 m apart, and well FW124 is located 1 m from the surface ERT line (Fig. 2d). Each borehole had 56 permanent electrodes, which were installed to be located primarily in the saturated section. The borehole electrode design was guided by the hydrogeological zonation described in Section 3. The vertical spacing between the electrodes was 0.6 m in the upper region (at depths less than 10 m) and 0.3 m in the more fractured lower region. For the borehole ERT, we used a bipole–bipole array that included dipoles of various lengths in either borehole or in both boreholes. Each cross-well dataset contained about 8500 data points, which included repeat and reciprocal measurements, and it took about 6 h to collect it. Similarly, to the surface acquisition, an optimal cross-well configuration would require only 3 h of recording without any loss of information of the subsurface. Again, reciprocal and repeat measurements that differed by more than 3% were removed from the data set, and data points with low current (<100 mA) and low voltage (<2 mV) were removed. Typically, about 10% of the data had an error larger than 3%, and about 20% of the data were removed because of low measured signals. We collected 22 cross-well datasets at various time intervals, spanning from fall 2008 through fall 2009 (Fig. 3).

We used stainless steel electrodes for both of the surface and cross-well ERT data acquisitions. Their favorable noise characteristics allow them to perform reasonably well for both resistivity and chargeability measurements, and their high durability underground makes them suitable for long-term monitoring applications (LaBrecque and Daily, 2008). Shallow borehole electrodes did not perform well because of poor contact with the surrounding unsaturated sediments. However, all wellbore electrodes located in the saturated zone performed well throughout the experiment. The average contact resistance for a surface array was 1000 Ω, with the area between x = 45 and 67 m having

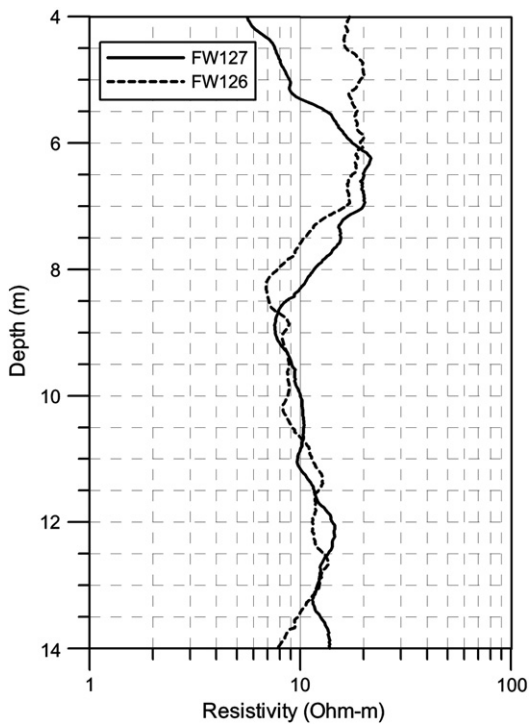

Fig. 4. Resistivity values as a function of depth from FW126 and 127 wells obtained by EM induction logging tool. The water table is at ~4–5 m below ground surface.

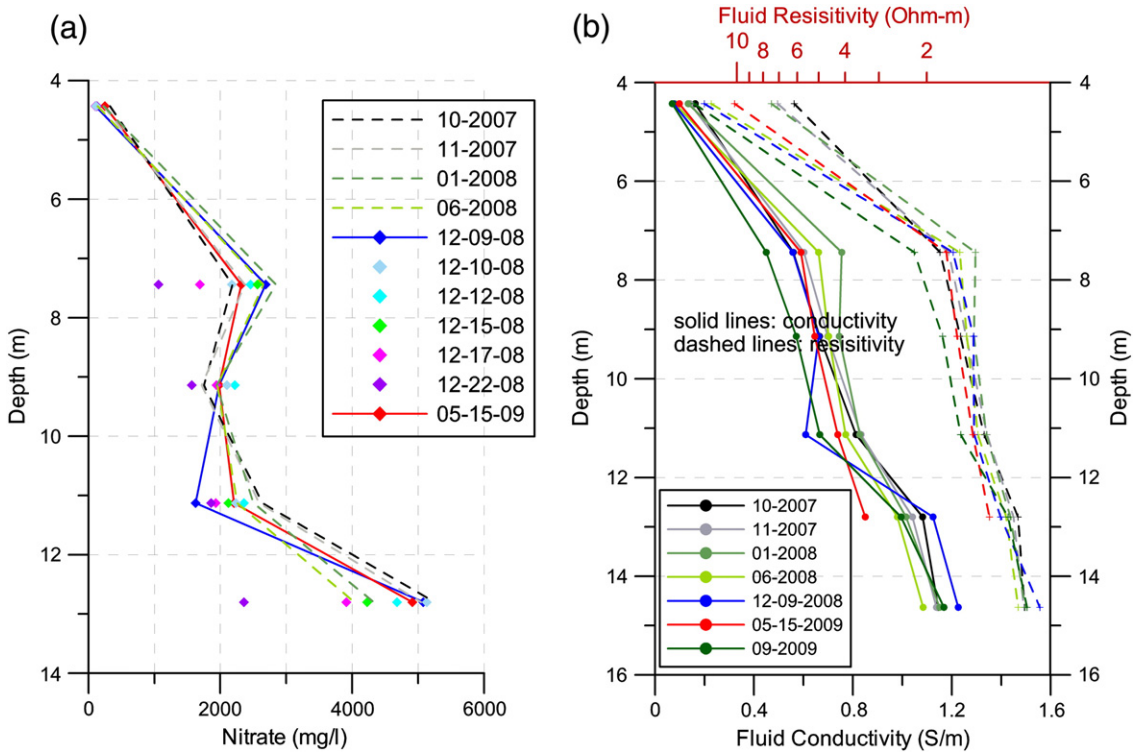

Fig. 5. (a) Nitrate concentration (mg/l), and (b) fluid conductivity (S/m) and resistivity (Ω-m) as a function of depth in FW120. Colors indicate different dates associated with acquisition campaigns. In Fig. 5b conductivities are plotted with solid lines while resistivities are plotted with dashed lines.

slightly higher values than the rest of the profile. The borehole electrodes had contact resistances below 1000 Ω for depths larger than 10 m, and 1000–3000 Ω for depths between 5 m and 10 m. The responses were stable and repeatable; no significant variations were observed with time (i.e., during a survey conducted on a single day).

Fig. 3 shows that while there were many cross-well and surface ERT data sets, only those acquired during four campaigns (December 9–12, 2008; December 20–24, 2008; May 12–13, 2009; and September 8–10, 2009) were coincident with geochemical sampling in the nearby wellbore FW120 (described below). In addition to these campaigns, surface and cross-well ERT data sets were collected within 1–2 days on December 1, 2008, July 23, 2009, and September 30, 2009.

4.3. EM induction wellbore measurements

Fig. 4 shows resistivities measured in wells FW126 and 127 (black diamonds in Fig. 2c and d) in October 2008 using a Mt. Sopris induction electromagnetic (EM) tool. These wells are 3 m apart, 3 m NW of wells FW124 and FW125 and 1.5 m NW of FW120. While the resistivity response in the upper (primarily variably saturated) 6 m is very different at these two wells, below this depth both curves show a resistivity decrease from 20 to 7 Ω-m at 6–10 m depth range, and a

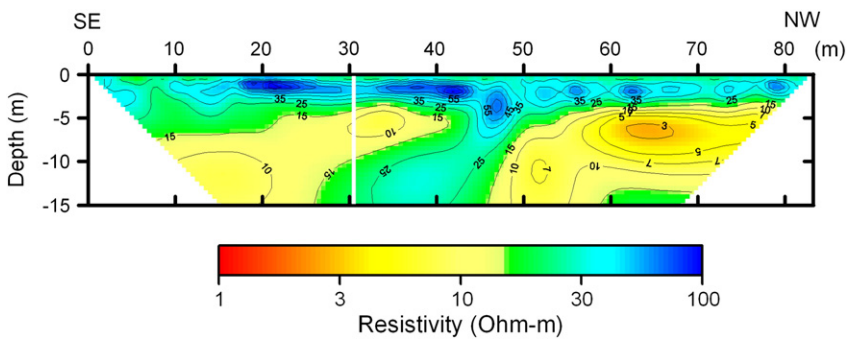

Fig. 6. Resistivity distribution recovered from surface ERT data collected on November 7, 2008, which was used as a reference model for successive time-lapse inversions. The white vertical line indicates the location of the borehole ERT array, which is downgradient and oriented perpendicular to the surface line.

resistivity increase to ~15 Ω-m in the deeper part of the wells (in the vicinity of the transition zone). Furthermore, the resistivity response is shifted by ~1 m, with FW127 being deeper and more resistive, which is consistent with the geological structure.

4.4. Precipitation measurements

Fig. 3 also shows daily and cumulative rainfall as a function of time. In 2008, a very dry summer (cumulative rainfall of 0.06 m vs. 0.43 m for the same time period in 2009) was followed by heavy storms in the winter. The cumulative rainfall in November 2008 was 0.1 m with two main storms — November 11–14 (with 0.05 m of rain) and November 28–30 (with 0.036 m of rain). December's cumulative rainfall was 0.2 m, with the heaviest storm occurring on December 9–12 (with 0.1 m of rain). The precipitation during 2009 was more typical for the region, with an average rainfall of 0.15 m per month in January and in May through September; the driest months were February (with 0.077 m of rain), and March and April (with 0.1 m of rain each month).

4.5. Geochemical and temperature measurements

A multilevel geochemical sampling well (FW120) having six different sampling depths between 4.5 m and 15 m is located close to the cross-well and surface ERT datasets (green circle in Fig. 2c and d), serving as a point of calibration for this study. Fluid samples were collected in the well on the days shown in Fig. 3. Groundwater measurements of specific conductance and temperature were made using a Troll 9500 apparatus in the field, and the corresponding fluid samples were subsequently assessed for nitrate by ion chromatography. Groundwater temperature measurements were performed after the samples had been brought to the surface and, as such, provide only an approximate measure of the groundwater temperature. However, the temporal temperature variations of these samples were minor (with average variations less than 1 °C and maximum variations from 1 to 2 °C). Additionally, in-situ groundwater temperature measurements from

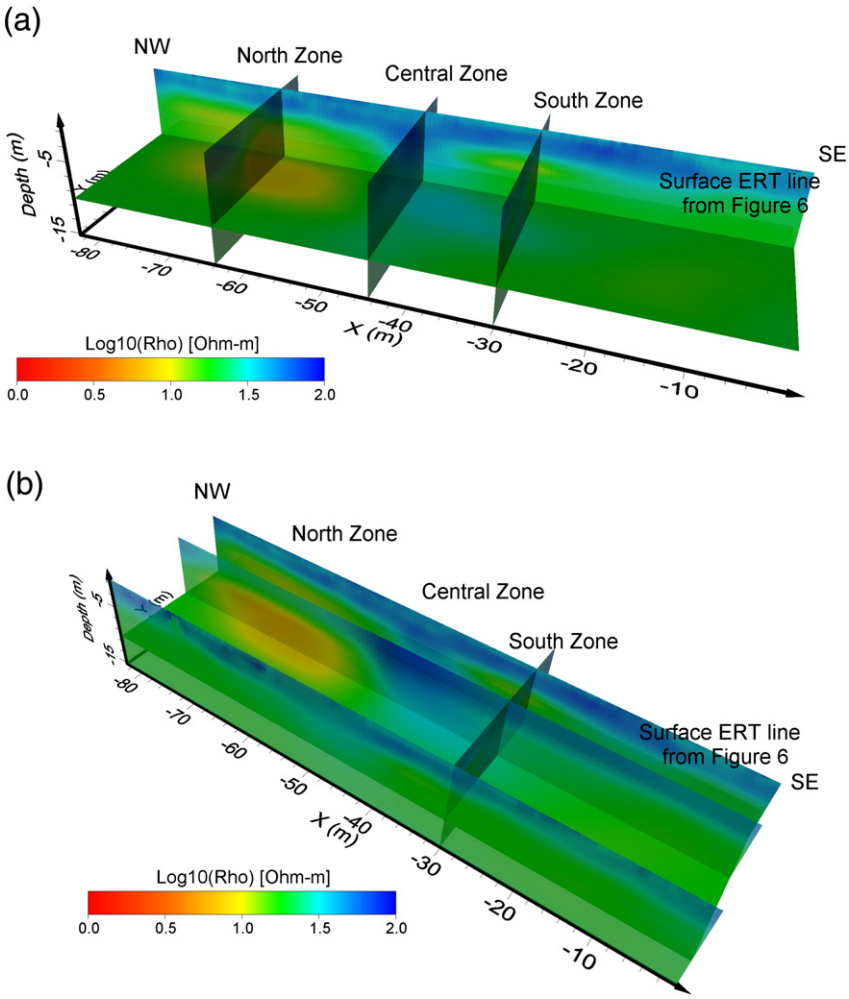

Fig. 7. Interpreted resistivity structure from 3D inversion of surface ERT data — (a) cutaway view through three distinct zones, and (b) side view showing variations downgradient from the ponds.

other parts of the study area show seasonal variations of only 2–3 °C. Using Eq. (6), these small variations would translate to only a 5–7% change in fluid resistivity. For example, a temperature increase of 2 °C would change fluid resistivity from 10 Ω-m to 9.5 Ω-m or from 1.6 Ω-m to 1.52 Ω-m. For these reasons, we assume that temperature variations in the groundwater have a negligible effect on the bulk resistivity, and thus we do not consider them in our interpretation.

Temporal variations in nitrate concentrations and fluid conductivity values in wellbore FW120 are shown in Fig. 5a and b. The shallow sampling ports reveal relatively low nitrate concentrations (~100 mg/l) and therefore relatively low fluid conductivity (~0.1 S/m). Samples extracted from sampling ports located between 7 and 12 m reveal nitrate concentrations of 2000 mg/l and conductivities of 0.4–0.8 S/m, while deeper samples reveal the highest nitrate concentrations (>4000 mg/l) and fluid conductivities (1.0–1.2 S/m). Data from October 2007 through June 2008 are also shown, although they were collected prior to our experiment. Note that nitrate concentrations were not collected in September 2009. In addition to showing fluid conductivity values, Fig. 5b shows the respective values of fluid resistivity for reference.

5. Interpretation of baseline electrical datasets

Surface and cross-well ERT baseline data sets were inverted independently following Eq. (2). We assumed Gaussian distribution of data errors of 3% and 7%, and initial values of Lagrange multiplier α of 10 and 500 for surface and cross-well, respectively, roughness parameter R = 0.2 for both kinds of data sets, and a horizontal-to-vertical roughness ratio equal to one for surface data sets, and larger than one for cross-well data sets, to allow for a stronger lateral resistivity variation. These parameters change iteratively during the inversion to obtain a solution that best fits the data, and we verified that inversion results were not affected by the choice of initial parameters. The baseline inversions and all subsequent time-lapse surface ERT inversions had an RMS misfit (Eq. (3)) of 3% and a normalized L2 = 1 (Eq. (4b)), while the cross-well ERT inversions had an RMS misfit of 7% and a normalized L2 = 1. These RMS values represent good estimates of noise in the data, as with lower noise values inversions would not converge and reach normalized L2 of one. Furthermore, RMS values are an indirect indication that numerical modeling errors are minimal, and appropriate inversion parameters were selected.

An interpretation of the gross hydrogeological-geophysical zonation was performed using the inverted baseline surface ERT dataset, collected on November 7, 2008, after a prolonged dry season. Fig. 6 shows the 2D electrical resistivity distribution obtained from the inversion of surface ERT data. The white vertical line indicates the projected intersection of the cross-well ERT array (which is offline and perpendicular to the surface array). Due to the extremely high nitrate concentration values in this region, we assume that the electrical response will be dominated by groundwater quality variations, which in turn may be influenced by hydrogeological and geological variations. Assessment of Fig. 6 reveals a ~4 m thick high-resistivity region corresponding to the vadose zone at the top part of the section; the base of this region coincides with the expected depth of the water table. In the deeper, saturated section, the electrical responses reveal three zones that vary laterally. The north (x > 50 m) and south (x = 0–35 m) zones have lower resistivity values (or higher conductivity values) relative to the central zone. Wellbore lithological data in the study area are sparse, although recent drilling at the north end of the ERT profile (near x = 64 m) reveals competent bedrock at a depth of 7 m. Comparison of this ERT baseline profile with seismic data collected at the same location by Watson et al. (2005; not shown) reveals that the central zone coincides with a low seismic P-wave velocity region. Projection of older and deeper wellbore lithological data onto the shallow seismic section suggests that the low velocity zone is coincident with a region having a greater proportion of weathered limestone relative to surrounding, less weathered shale units (Gaines, 2011). This comparison suggests that the laterally varying resistivity zones evident on the ERT profile shown in Fig. 6 may represent three lithologically distinct zones that influence plume spatial distribution: a central zone that is weathered

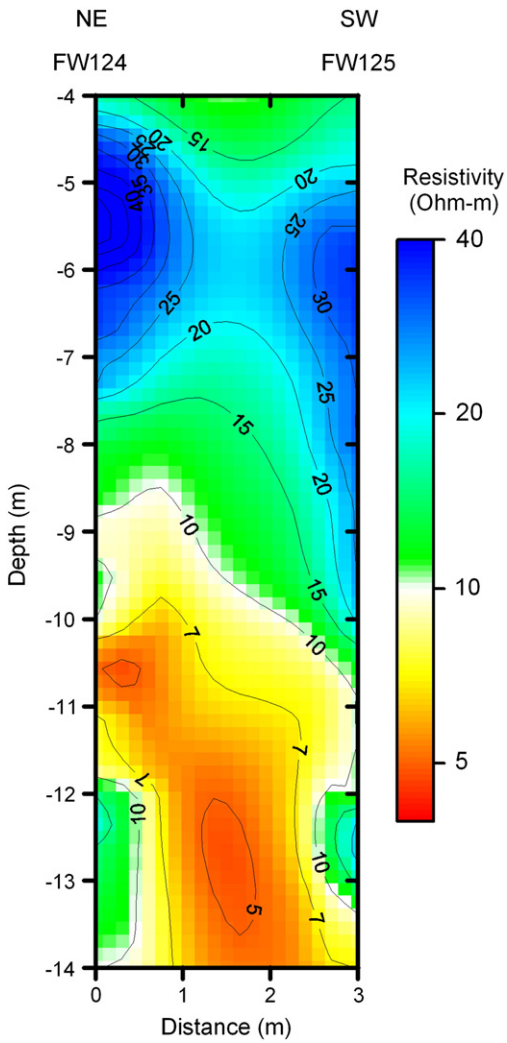

Fig. 8. Resistivity distribution recovered from cross-well ERT data collected on November 11, 2008, which was used as a reference model for successive time-lapse inversions.

limestone, surrounded by south and north zones that are more shale rich. Supporting the stratigraphic control concept, Watson et al. (2005) found that wellbore measurements from a wellbore located near x = 70 m and at a depth of 7–8 m, corresponding to the region of lowest resistivity in Fig. 6, revealed some of the highest nitrate concentration values in the region.

To investigate the persistence of the observed zonation in the geological strike direction, we collected surface ERT data along three parallel profiles during a single acquisition

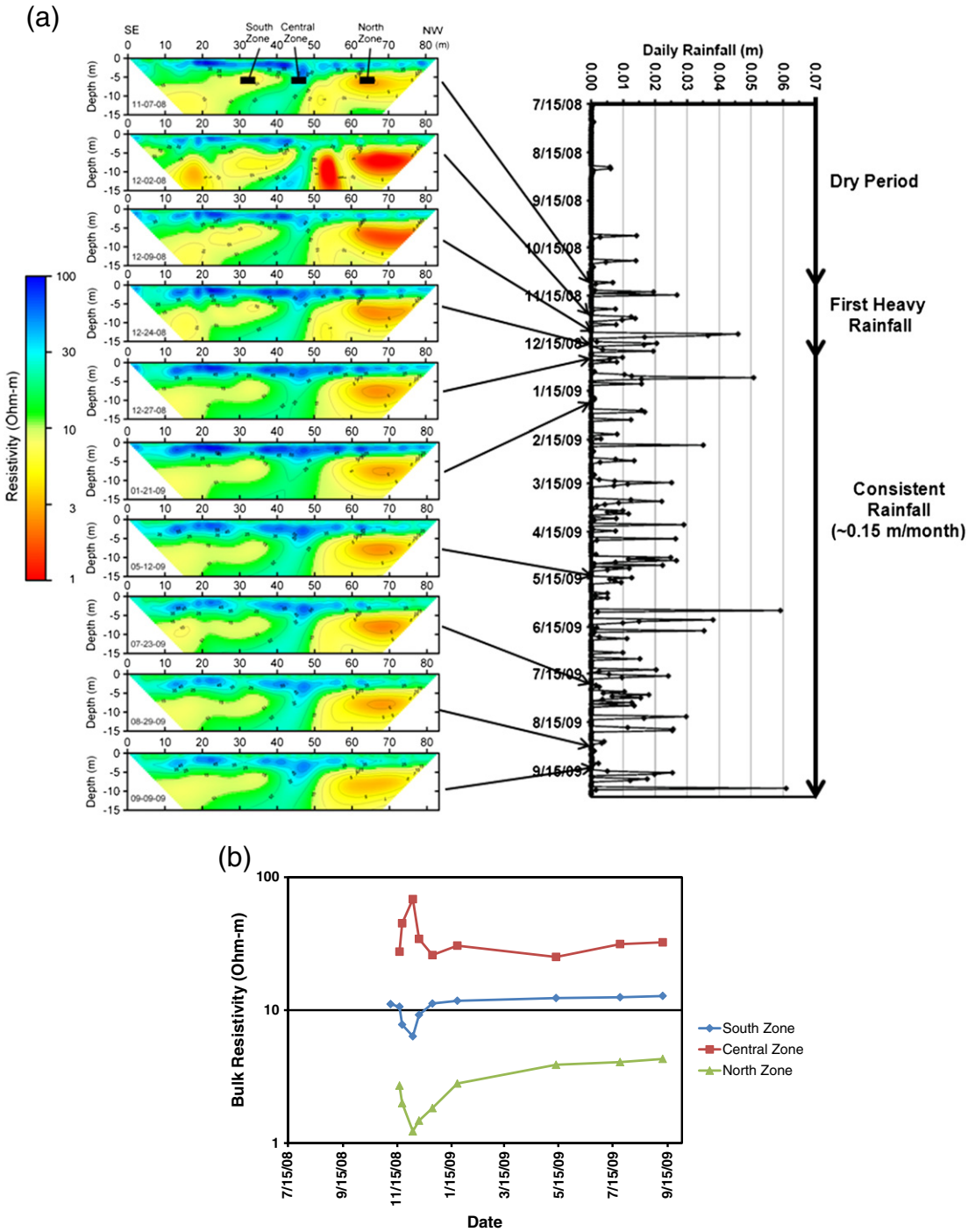

Fig. 9. (a) Resistivity distribution recovered from surface ERT data at 10 different times from November 7, 2008 to September 9, 2009 compared to rainfall. (b) Bulk resistivity as a function of time for three zones indicated by black squares in the upper plot of Fig. 9a.

campaign in March 2010 (blue dashed lines in Fig. 2c). One of the profiles was our long-term monitoring surface profile described above; one profile was located 5 m closer to the basin and the other profile was located 20 m downgradient. Individual 2D inversions (not shown) and a 3D inversion of this dataset (Fig. 7) revealed a zonation similar to that described above, although it suggests that the resistivity values in the north zone are not as low downgradient from the basin. Although wellbore confirmation distributed along the profile is lacking, this dataset, together with findings from the Gaines (2011) and Watson et al. (2005) studies, suggests that the dipping and variable lithology along the profile influence plume distribution near the S-3 ponds.

We also interpret the baseline cross-well ERT in terms of local hydrogeology. Fig. 8 shows the electrical resistivity distribution obtained from the inversion of cross-well ERT data collected on November 11, 2008. Cross-well ERT inversions cover only the saturated portion of the profile, because data from electrodes in the unsaturated zone were noisy and therefore excluded from interpretation. As described by Kowalsky et al. (2011), based on comparison with wellbore lithological data, the tomogram can be divided vertically into three geological zones that are reflected by electrical zonation: an upper saprolite layer (4–7 m), a lower saprolite layer (7–9 m), and a transition zone (below 9 m). Lithological analysis of wellbore FW120 (near x = 35 m) suggests the presence of a more highly weathered and fractured transition zone at a depth of about 10 m (Kowalsky et al., 2011). 2D resistivity inversion shows an apparent not a true dip due to 3D effects and current channeling, since the wells are in the direction of the fluid flow. A comparison of Figs. 6 and 8 reveals that while the cross-well array is very sensitive to local-scale vertical heterogeneities, the surface ERT instead provides good information about gross lateral zonation.

Although we expect discrepancies between the direct comparison of the local cross-well ERT and the surface ERT responses because they have different measurement support scales, are offset in space, are oriented differently relative to geologic dip, and from other supporting information we

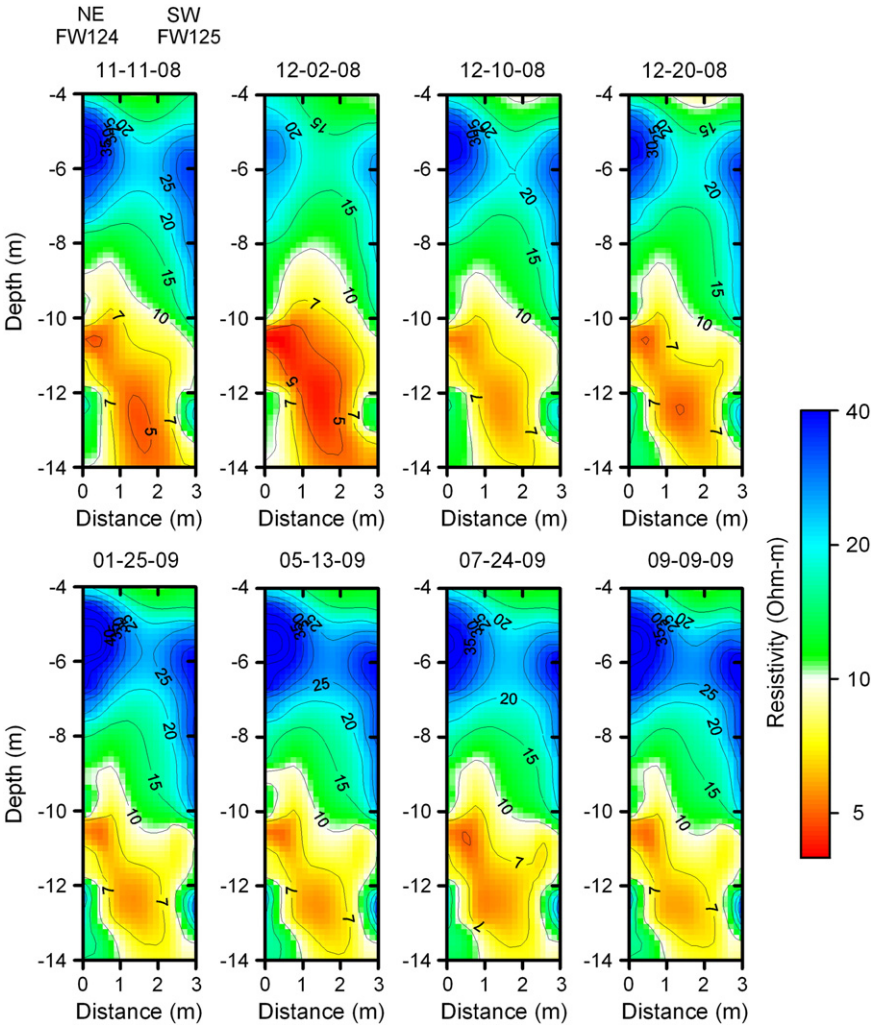

Fig. 10. Resistivity distribution recovered from cross-well ERT data at eight different times from November 11, 2008 to September 9, 2009.

know that the geology is 3D, or anisotropic, it is useful to compare responses where the profiles are most closely co-located (or near the white line in Fig. 6). We find that upon comparison, and after compensating for dip and offset, while there is a 20–30% difference in the inverted baseline resistivity values, the structural patterns agree very well. Although new codes that allow for a sharp resistivity change across the boundaries or anisotropy would likely improve this comparison, we contend that the comparison is acceptable for our purposes of using time-lapse ERT datasets to explore recharge-induced nitrate dilution. In areas where wells might not be available or there is a need for a noninvasive monitoring method, surface ERT could help identify areas for further investigations.

6. Interpretation of Time-Lapse ERT

Time-lapse surface and cross-well ERT baseline data sets were inverted independently at each time, following Eq. (2), and also in a time-lapse mode (LaBrecque and Yang, 2001). The model obtained from the inversion of the initial data set was used as a reference model to constrain the inversion of the subsequent time-lapse datasets. We also compared the time-lapse inversions to differences between inversions at each time and the results were very similar.

Fig. 9 illustrates selected surface ERT profiles collected during the year on the left and daily rainfall on the right. Recharge is expected to change the moisture and temperature of the vadose zone region (at depths less than 4 m) as well as the groundwater geochemistry as was discussed in Section 4. Although we focus here on interpretation of precipitation-induced changes to resistivity and geochemistry in the saturated zone, Gasperikova et al. (2010) showed that resistivity variations in the vadose zone between May and September 2009 were on the order of 15–25%, based on these surface ERT datasets. To illustrate temporal variations in resistivities due to precipitation, Fig. 9a shows surface ERT inversions along the profile as a function of depth at ten different times. The measurements for our reference model were made on November 7, 2008, which represents conditions after a long dry season. In general, the three lithologically distinct zones identified on the baseline surface ERT profile (Fig. 6) remain distinct on the subsequent monitoring datasets (south zone from ~0 to 35 m; central zone from ~35 to 50 m; north zone from >50 m). Comparison of the monitoring datasets suggests that the most pronounced change in electrical resistivity in both the north and south zones was associated with the profile collected during the first large December 2008 storms that followed a long dry spell. During this period, the resistivity decreased dramatically in the north zone and moderately in the south zone. The central zone, which is interpreted to be a weathered limestone zone as described earlier, appears to have consistently higher resistivity values.

To highlight how electrical resistivity changes as a function of these three lithological-based zones over time (and thus with rainfall), we examine the resistivity time series associated with three shallow groundwater locations located in the different zones, as shown by black squares in the upper ERT profile in Fig. 9a. The time-series of electrical resistivity associated with each of these locations are shown in Fig. 9b. Fig. 9b shows that the more shale-rich north and south zones of the profile respond similarly to precipitation, with an initial decrease in resistivity associated with the first storms of the season of up to 50–70% of baseline values. In contrast, the resistivity in the central zone, which is interpreted to be weathered limestone, is generally higher than the shale-rich regions and increases up to 55% of baseline values with the first storms of the season. With continued rainfall, the resistivity values of all three zones revert approximately to baseline conditions.

Fig. 10 shows the variations in the responses from cross-well ERT inversions during the same period. Again, the onset of heavy storms in early December produced the largest decrease in the resistivities, while the responses are very similar from the end of December 2008 until September 2009. Although the control of gross zonation on the electrical response to recharge is not evident on the along-strike local-scale ERT tomograms, these data also illustrate that the greatest changes in electrical resistivity are evident during the December "wetting up" period.

7. Interpretation of ERT datasets in terms of nitrate plume response to recharge

The discussions above have illustrated that ERT responses vary in a systematic way to recharge events, suggesting that

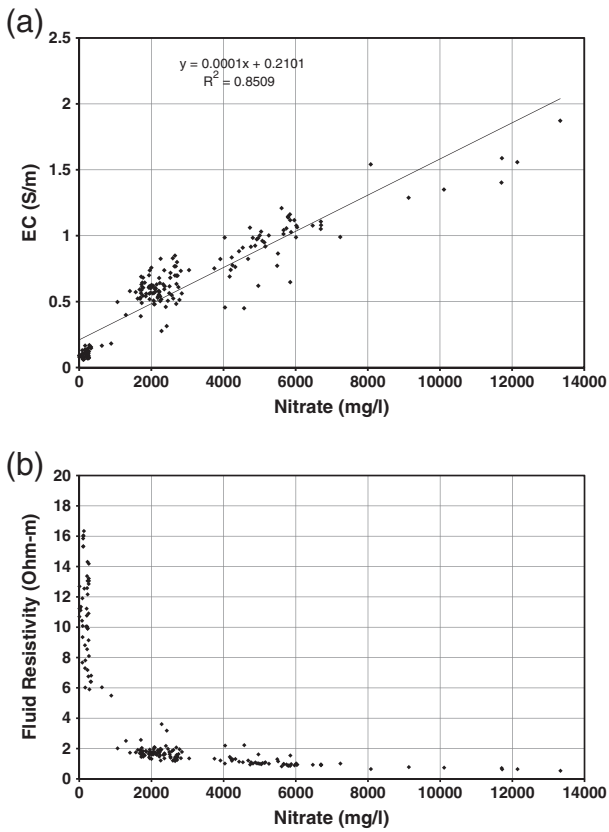

Fig. 11. (a) Fluid electrical conductivity (S/m) and (b) fluid electrical resistivity (Ω-m) as a function of nitrate concentration (mg/l) in wells near FW120. Black symbols indicate groundwater measurements, and black line in (a) is the best fit described by the equation at the top left.

these data are potentially useful for exploring recharge-induced plume dynamics. To explore the magnitude of groundwater nitrate variations with recharge, we first develop petrophysical relationships that take advantage of Archie's law (Eq. (5)) and site-specific relationships between fluid electrical conductivity and nitrate concentration developed using wellbore geochemical data from FW120 and wells nearby. We recognize that the petrophysical relationships developed at this location may not be stationary across the site (Day-Lewis et al., 2005; Singha and Moysey, 2006); we especially expect them to vary in the downgradient direction (i.e., away from the plume source). However, we assume that the relations developed at FW120 are valid for use with the monitoring surface ERT transect, which is located equidistant from the edge of the seepage basin.

We make two assumptions when we invoke Eq. (5) to estimate nitrate concentrations from the ERT data. First, we assume that seasonal temperature variations (Section 4.5) have a negligible effect on the resistivity response compared to changes in bulk resistivity due to rainfall (Fig. 9b). Second, we assume that surface conduction in the saprolite layer does not change much over time, and its contribution to the overall response is much smaller than changes in the transition zone. The wellbore geochemical datasets in the saturated section indicate that nitrate represents by far the largest contributor to the groundwater TDS. As shown in Fig. 11b, we also find that fluid electrical resistivity decreases asymptotically as the nitrate concentration increases. Fig. 11b suggests that at this site we can expect the ERT data to be able to detect rainfall-associated changes in nitrate concentration if they occur in the range of 100–2000 mg/l. However, ERT is expected to be relatively insensitive to changes in nitrate concentration on the order of 10–20 mg/l that occur when concentrations are less than 100 mg/l. At high concentration ranges (>2000 mg/l), significant changes in nitrate concentration (~1000 mg/l) are required in order to be electrically detectable. The asymptotic resistivity behavior shown in Fig. 5b may therefore cause high nitrate concentrations to be underestimated.

Fig. 12 illustrates that a 20–60% decrease in nitrate concentrations (Fig. 5) between December 9 and 22 through the whole depth profile corresponds to an 18–36% increase in surface ERT resistivity, and these changes are easily detectable by surface ERT. The changes observed during the rain events in December are short lived; the response quickly returns to background values. We have observed similar behavior of ERT responses due to rainfall events in July and September 2009, but have no geochemical measurements to

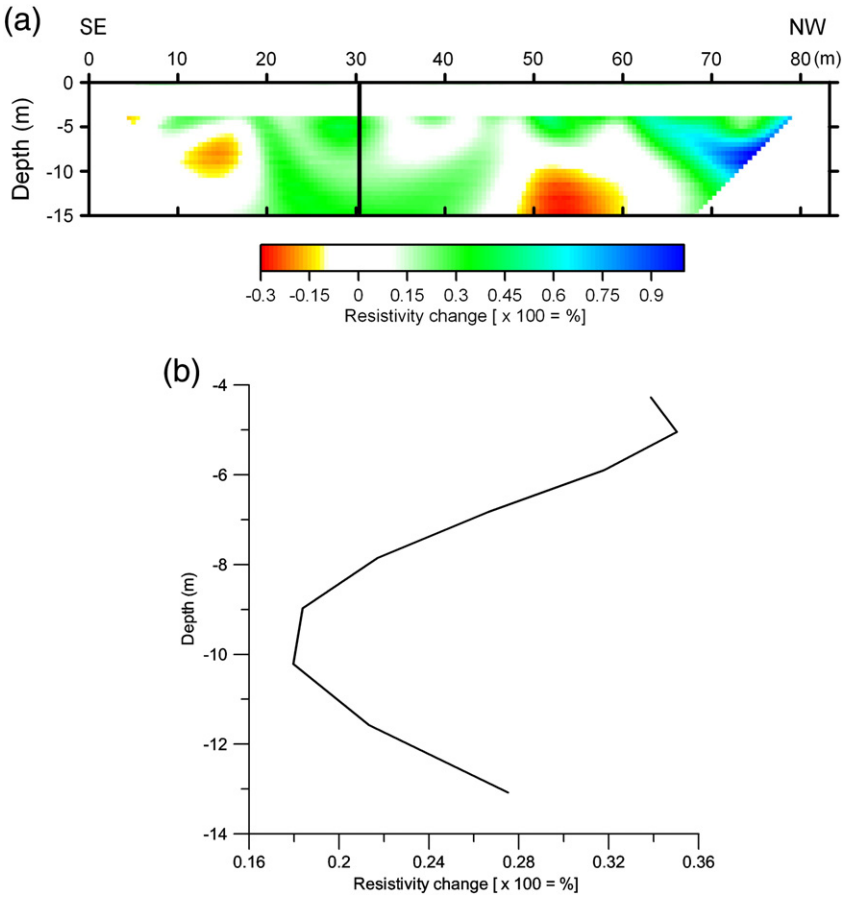

Fig. 12. (a) Resistivity change between December 9 and December 24 along the surface ERT profile, (b) resistivity change as a function of depth at the FW124 well. Positive values indicate resistivity increase while negative values indicate resistivity decrease with respect to December 9 response.

confirm it. Smaller variations in nitrate concentrations related to seasonal changes are not detectable by surface ERT.

To invoke Archie's law to estimate nitrate concentrations from the ERT-based bulk resistivity values, we rely on hydraulic properties estimated by Kowalsky et al. (2011), although we combine values associated with the deeper units to account for the coarser measurement support scales of the surface ERT relative to the cross-well ERT. Porosities used for the fill, upper saprolite, and combined lower saprolite and the transition zone were 0.15, 0.36 and 0.25, respectively, and the values for Archie's coefficient m were 1.68, 1.68, and 1.27, respectively. These values were used with the site-specific relationship shown in Fig. 11 and the inverted resistivity distributions to estimate nitrate concentrations over time, which were then compared to nearby wellbore values (Fig. 5).

Using the approach described above, Fig. 13a shows the measured nitrate concentration as a function of depth in FW120 well for five different times in December 2008 and May 2009. At this wellbore location, the nitrate concentrations at the shallow depth are lower (~100 mg/l), between 7 and 11 m depth are around 2000 mg/l, and the deepest sample depth shows nitrate concentrations decreasing from 5000 mg/l (December 9) to ~2000 mg/l (December 22). Estimated concentrations from resistivities obtained by the nearby cross-well ERT inversions in December 2008 and May 2009 are shown in Fig. 13b. Accounting for some depth offset between FW120 and FW124, the estimated nitrate concentrations from the cross-well ERT reflect the borehole nitrate concentration range and vertical trends quite well, with lower nitrate concentrations at the top of the saturated section and higher values near the base of the imaged section. Over the time period shown, the crosswell and wellbore data both demonstrate a decrease in nitrate at ~7.5 m and an increase in nitrate at ~11 m, with little change at 4.5 m and 13 m.

Fig. 13c shows the interpretation of nitrate distribution from surface ERT inversions for the same two time periods shown in Fig. 13b. As expected, we see that the north side of the profile has extremely high nitrate concentrations and the central zone has the lowest values. Compared to existing wellbore geochemical measurements, areas with high nitrate concentration (>2000 mg/l) are located correctly using surface ERT inversions, although the values are slightly underestimated, which is attributed to the fact that estimated resistivity from surface ERT corresponds to a larger volume being sampled. Also, surface ERT data are not sensitive to further resistivity decrease at depth as shown by cross-well inversions. Although there are no

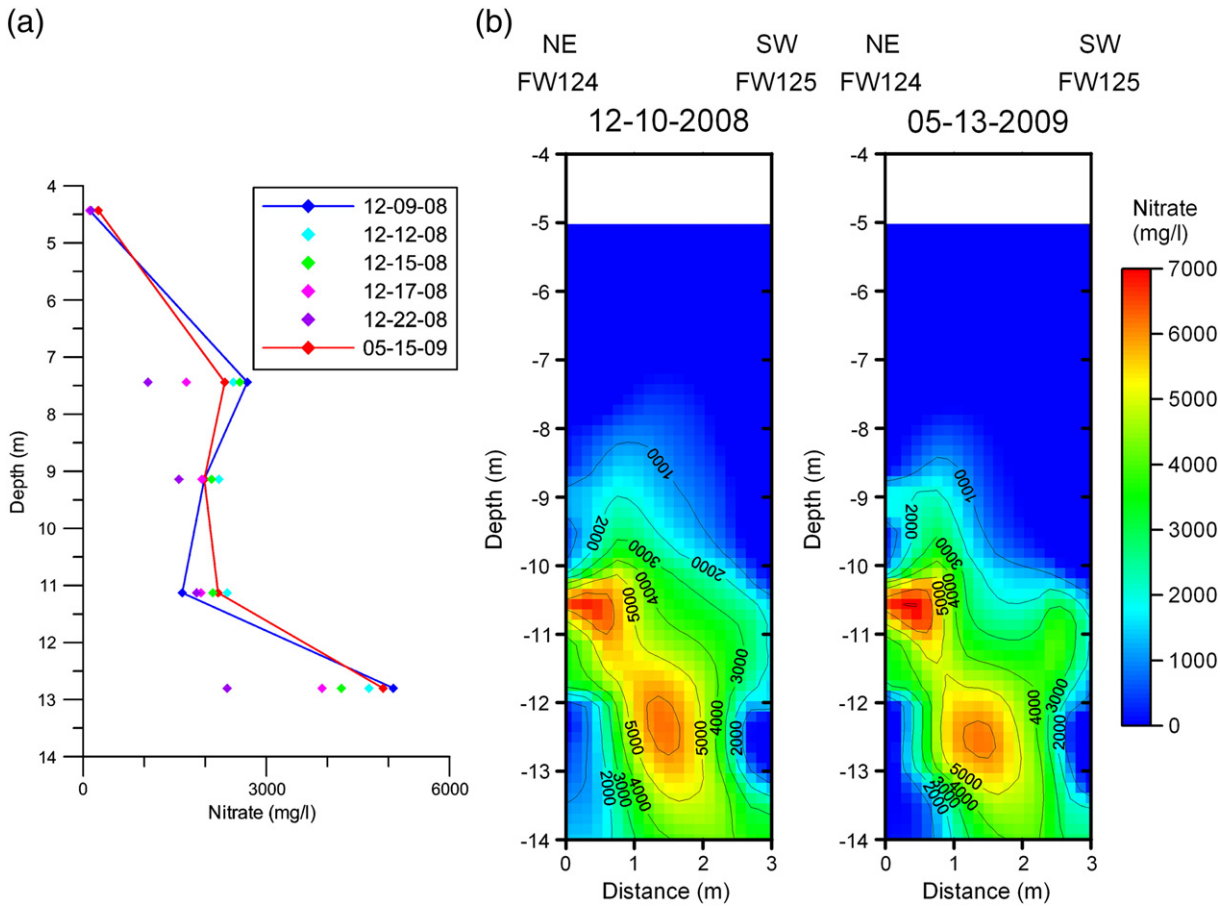

Fig. 13. (a) Measured nitrate concentrations (mg/l) in FW120 for six different dates (b) nitrate concentrations (mg/l) estimated from cross-well ERT data at two of the six dates shown in Fig. 13a, and (c) nitrate concentrations estimated using surface ERT inversions for the same two dates.

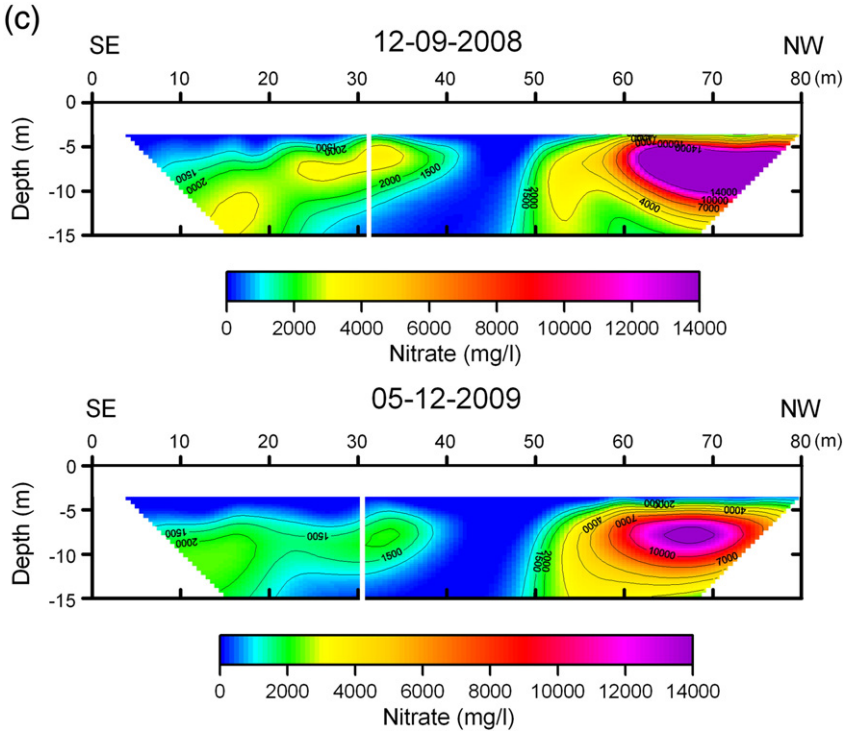

Fig. 13 (*continued*).

time-coincident wellbore nitrate concentration data to validate the ERT-derived nitrate concentration interpretation on the north end of the profiles, the generally higher values shown are consistent with those described by Watson et al. (2005) near x = 70 m of 42,000 mg/l.

This study illustrates that cross-well ERT gives the most detailed information about the subsurface in the wells' vicinity. As surface ERT arrays in 2D and 3D increase, the resolution decreases. However, surface ERT provides a very important discrimination capability between areas of low and high nitrate concentrations. Surface ERT interpretation can be improved by including any available cross-well ERT data and their spatial distribution function, or seismic information as a-priori information.

We find that the central zone appears to be more susceptible to quick nitrate dilution with recharge, whereas the north and south zones appear to either release nitrate from the matrix into pore spaces or to preferentially receive more incoming nitrate from the basins upon first rainfall events. These results support the notion that lithologically based zonation likely influences the plume response to recharge at the site, and that the most significant change in resistivity over the course of this study occurred when significant rainfall followed an extended dry period.

8. Conclusions

Analysis of a large number of surface and cross-well ERT datasets collected over 12 months adjacent to the Oak Ridge IFRC S-3 ponds allowed us to gain insight into the relationship between resistivity responses and subsurface plume dynamics associated with natural episodic, and annual recharge and infiltration processes at a severely contaminated site. We found that the system response to short-term heavy rainstorms was different from the response to seasonal and annual fluctuations, and that there was good agreement between resistivity distributions recovered from cross-well and surface ERT data. In addition to the control of antecedent conditions, we interpret that hydrological zonation is a key control on the nitrate plume response to recharge.

The results at this site suggest that ERT datasets can potentially be used to interpret spatiotemporal variations in subsurface plume dynamics. While our earlier research at the site illustrated the value of coupled hydrogeophysical–geochemical inversion for parameter estimation and recharge process investigation at the local scale using cross-well ERT (Kowalsky et al., 2011), this study illustrates the value of a simple surface ERT interpretation approach for gaining insight about the role of hydrogeology and antecedent conditions on recharge-induced nitrate behavior over plume-relevant scales and on expected resolution that can be achieved with both cross-well and surface datasets. The utility of ERT datasets for such monitoring is dependent on the relationship between resistivity and nitrate concentration; at ORNL the ERT data were useful for identifying recharge-induced changes in nitrate concentrations that occurred in the 100–2000 mg/l range, but were insensitive to further resistivity decrease at depth due to the asymptotic

resistivity behavior at high nitrate concentrations. Ongoing research is focused on expanding the study to explore recharge-induced dynamics at the leading edge of the plume using time-lapse ERT, on understanding how recharge may also impact other geochemical variations that could contribute to complex electrical signatures (i.e., Skold et al., 2011), and on using the information obtained by geophysics to parameterize and validate reactive transport models that are being performed to simulate long term plume behavior (i.e., Tang et al., 2010).

Acknowledgments

This work was supported by the U.S. Department of Energy, Contract No. DE-AC02-05CH11231 and by the Subsurface Biogeochemical Research Program of the U.S. DOE Office of Biological and Environmental Research as part of the Oak Ridge National Laboratory IFRC Study. The authors would like to thank Marcella Mueller (ORNL) for assistance with the hydrogeochemical data, and two anonymous reviewers for suggestions and comments that helped us to improve this manuscript.

References

Archie, G.E., 1942. The electrical resistivity log as an aid in determining some reservoir characteristics. Transactions of AIME 146, 54–62.

Binley, A., Cassiani, G., Middleton, R., Winship, P., 2002. Vadose zone flow model parameterization using cross-borehole radar and resistivity imaging. Journal of Hydrology 267, 147–159.

Brooks, S., 2001. Waste characteristics of the former S-3 Ponds and outline of uranium chemistry relevant to NABIR field research studies. http://www.ornl.gov/~webworks/cppr/y2002/rpt/109994.pdf (ORNL/TM-2001/27).

Chambers, J.E., Loke, M.H., Ogilvy, R.D., Meldrum, P.I., 2004. Noninvasive monitoring of DNAPL migration through a saturated porous medium using electrical impedance tomography. Journal of Contaminant Hydrology 68, 1–12.

Chen, J., Hubbard, S.S., Peterson, J., Williams, K., Fienen, M., Jardine, P., Watson, D., 2006. Development of a joint hydrogeophysical inversion approach and application to a contaminated fractured aquifer. Water Resources Research 42, W06425. http://dx.doi.org/10.1029/2005WR004694.

Chen, J., Hubbard, S.S., Korneev, V., Gaines, D., Baker, G., Watson, D., 2010. Stochastic inversion of seismic refraction data for estimating watershed-scale aquifer geometry: development and application to a contaminated aquifer. Water Resources Research 46, W11539. http://dx.doi.org/10.1029/2009WR008715 (16 pp.).

Commer, M., Newman, G.A., Williams, K.H., Hubbard, S.S., 2011. 3D induced-polarization data inversion for complex resistivity. Geophysics 76, F157–F171.

Constable, S.C., Parker, R.L., Constable, C.G., 1987. Occam's inversion: a practical algorithm for generating smooth models from electromagnetic sounding data. Geophysics 52, 289–300. http://dx.doi.org/10.1190/1.1442303.

Daily, W.D., Ramirez, A.L., 1995. Electrical resistance tomography during in-situ trichloroethylene remediation at the Savannah River site. Journal of Applied Geophysics 33, 1429–1442.

Daily, W.D., Ramirez, A.L., 2000. Electrical imaging of engineered hydraulic barriers. Geophysics 65, 83–94.

Daily, W., Ramirez, A., LaBrecque, D., Nitao, J., 1992. Electrical resistivity tomography of vadose water movement. Water Resources Research 28, 1429–1442. http://dx.doi.org/10.1029/91WR03087.

Daily, W., Ramirez, A., Binley, A., LaBrecque, D., 2004a. Electrical resistance tomography. The Leading Edge 23, 438–442. http://dx.doi.org/10.1190/1.1729225.

Daily, W., Ramirez, A., Binley, A., 2004b. Remote monitoring of leaks in storage tanks using electrical resistance tomography: application at the Hanford Site. Journal of Environmental and Engineering Geophysics 9, 11–24. http://dx.doi.org/10.4133/JEEG9.1.11.

Day-Lewis, F., Singha, K., Binley, A.M., 2005. Applying petrophysical models to radar travel time and electrical resistivity tomograms: resolution-dependent limitations. Journal of Geophysical Research 110, B08206.

Fishman, M.J., Friedman, L.C., 1989. Methods of determination of organic substances in water and fluvial sediments. Techniques of Water-Resource Investigations of the U.S. Geological Survey (Book 5, Chapter A1).

French, H.K., Hardbattle, C., Binley, A., Winship, P., Jakobsen, L., 2002. Monitoring snowmelt induced unsaturated flow and transport using electrical resistance tomography. Journal of Hydrology 267, 273–284.

Gaines, D.P., 2011. Advances in seismic first-arrival time tomography. University of Tennessee Master's Thesis, http://trace.tennessee.edu/utk_graddiss/972/.

Gasperikova, E., Kowalsky, M.B., Hubbard, S.S., Peterson, J.E., Baker, G.S., Smith, M., Watson, D.B., 2010. Long Term Time Lapse Surface and Borehole Electrical Resistivity Monitoring of Natural Recharge Induced Contaminant Plume Behavior: SEG Expanded Abstracts, 29, pp. 3930–3934.

Hatcher Jr., R.D., Lemiszki, P.J., Dreier, R.B., Ketelle, R.H., Lee, R.R., Leitzke, D.A., McMaster, W.M., Foreman, J.L., Lee, S.Y., 1992. Status Report on the Geology of the Oak Ridge Reservation. (ORNL/TM-12074) Martin Marietta Energy Systems, Oak Ridge, Tennessee.

Hayley, K., Bentley, L.R., Gharibi, M., Nightingale, M., 2007. Low temperature dependence of electrical resistivity: implications for near surface geophysical monitoring. Geophysical Research Letters 34, L18402. http://dx.doi.org/10.1029/2007GL031124.

Keller, G.V., Frischknecht, F.C., 1996. Electrical Methods in Geophysical Prospecting. Pergamon, London.

Kemna, A., Vanderborght, J., Kulessa, B., Vereecken, H., 2002. Imaging and characterization of subsurface solute transport using electrical resistivity tomography (ERT) and equivalent transport models. Journal of Hydrology 267, 125–146.

Koch, K., Wenninger, J., Uhlenbrook, S., 2009. Joint interpretation of hydrological and geophysical data: electrical resistivity tomography from a process hydrological research site in the Black Forrest Mountains, Germany. Hydrological Processes 23, 1397–1536.

Kowalsky, M.B., Gasperikova, E., Finsterle, S., Watson, D., Baker, G., Hubbard, S.S., 2011. Coupled modeling of hydrogeochemical and electrical resistivity data for exploring the impact of recharge on subsurface contamination. Water Resources Research 47, W02509. http://dx.doi.org/10.1029/2009WR008947.

LaBrecque, D., Daily, W., 2008. Assessment of measurement errors for galvanic-resistivity electrodes of different composition. Geophysics 73, F55–F64.

LaBrecque, D., Yang, X., 2001. Difference inversion of ERT data: a fast inversion method for 3-D in situ monitoring. Journal of Environmental and Engineering Geophysics 6, 83–89. http://dx.doi.org/10.4133/JEEG6.2.83.

Miller, C.R., Routh, P.S., Brosten, T.R., McNamara, J.P., 2008. Application of time-lapse ERT imaging to watershed characterization. Geophysics 73, G7–G17.

Oldenborger, G.A., Knoll, M.D., Routh, P.S., LaBrecque, D.J., 2007. Time-lapse ERT monitoring of an injection/withdrawal experiment in a shallow unconfined aquifer. Geophysics 72, F177–F187.

Park, S.K., 1998. Fluid migration in the vadose zone from 3-D inversion of resistivity monitoring data. Geophysics 63, 41–51.

Ramirez, A., Daily, W., LaBrecque, D., Owen, E., Chesnut, D., 1993. Monitoring an underground steam injection process using electrical resistance tomography. Water Resources Research 29, 73–87.

Ramirez, A., Daily, W., Binley, A., LaBrecque, D., Roelant, D., 1996. Detection of leaks in underground storage tanks using electrical resistance methods. Journal of Environmental and Engineering Geophysics 1, 189–203. http://dx.doi.org/10.4133/JEEG1.3.189.

Rein, A., Hoffmann, R., Dietrich, P., 2004. Influence of natural time-dependent variations of electrical conductivity on DC resistivity measurements. Journal of Hydrology 285, 215–232. http://dx.doi.org/10.1016/j.jhydrol.2003.08.015. ISSN 0022–1694, http://www.sciencedirect.com/science/article/pii/S0022169403003226.

Revil, A., Skold, M., Hubbard, S.S., Wu, Y., Watson, D.B., and Karaoulis, M., in press. Petrophysical properties of saprolite from the Oak Ridge Integrated Field Research Challenge site, Tennessee. Geophysics.

Roden, E., Scheibe, T., 2005. Conceptual and numerical model of uranium(VI) reductive immobilization in fractured subsurface sediments. Chemosphere 59, 617–628.

Singha, K., Gorelick, S.M., 2005. Saline tracer visualized with three-dimensional electrical resistivity tomography: field-scale spatial moment analysis. Water Resources Research 42, W05023. http://dx.doi.org/10.1029/2004WR003460.

Singha, K., Moysey, S., 2006. Accounting for spatially variable resolution in electrical resistivity tomography through field-scale rock physics relations. Geophysics 71, A25–A28.

Skold, M., Hubbard, S.S., Karaoulis, M., Revil, A., Spycher, N., Watson, D., Wu, Y., 2011. Coupled interpretation of geoelectrical surveying results in environmental site investigations. AGU Fall Meeting, San Francisco, CA.

Slater, L., Binley, A., 2003. Evaluation of permeable reactive barrier (PRB) integrity using electrical imaging methods. Geophysics 68, 911–921.

Slater, L., Binley, A., Versteeg, R., Cassiani, G., Birken, R., Sandberg, S., 2002. A 3D ERT study of solute transport in a large experimental tank. Journal of Applied Geophysics 49, 211–229.

Solomon, D.K., Moore, G.K., Toran, L.E., Dreier, R.B., McMaster, W.M., 1992. Status Report: A Hydrologic Framework for the Oak Ridge Reservation. (ORNL/TM-12026) Oak Ridge National Laboratory, Oak Ridge, TN.

Spalding, R.F., Exner, M.E., 1993. Occurrence of nitrate in groundwater—a review. Journal of Environmental Quality 22, 392–402.

Tang, G., D'Azevedo, E., Zang, F., Parker, J., Watson, D.B., Jardine, P.M., 2010. Application of a hybrid MPI/OpenMP approach for parallel groundwater model calibration using multi-core computers. Computers & Geosciences 36, 1451–1460.

Telford, W.M., Geldart, L.P., Sheriff, R.E., 1990. Applied Geophysics. Cambridge University Press, pp. 522–577.

U.S. Department of Energy, 1997. Report on the Remedial Investigation of Bear Creek Valley at the Oak Ridge Y-12 Plant, Oak Ridge, Tennessee. (DOE/OR/01–1455/V1&D2) Department of Energy, Oak Ridge, Tennessee.

U.S. Environmental Protection Agency, 2005. Drinking Water Regulations and Health Advisories. Office of Water, Washington, D.C.

Van der Hoven, S.J., Solomon, D.K., Moline, G.R., 2005. Natural spatial and temporal variations in groundwater chemistry in fractured, sedimentary rocks: scale and implications for solute transport. Applied Geochemistry 20, 861–873. http://dx.doi.org/10.1016/j.apgeochem.2004.11.013.

Ward, A.S., Gooseff, M.N., Singha, K., 2010. Imaging Hyporheic Zone Solute Transport using Electrical Resistivity. Hydrological Processes, 24. John Wiley & Sons, Ltd, pp. 948–953. http://dx.doi.org/10.1002/hyp.7672.

Watson, D.B., Doll, W.E., Gamey, T.J., Sheehan, J.R., Jardine, P.M., 2005. Plume and lithologic profiling with surface resistivity and seismic tomography. Ground Water 43, 169–177. http://dx.doi.org/10.1111/j.1745-6584.2005.0017.x.

Wu, W., Carley, J., Fienen, M., Mehlhorn, T., Lowe, K., Nyman, J., Luo, J., Gentile, M.E., Rajan, R., Wagner, D., Hickey, R.F., Gu, B., Watson, D., Cirpka, O.A., Kitanidis, P.K., Jardine, P.M., Criddle, C.S., 2006. Pilot-scale in situ bioremediation of uranium in a highly contaminated aquifer. 1. Conditioning of a treatment zone. Environmental Science and Technology 40, 3978–3985.

Wu, W., Carley, J., Green, S.J., Luo, J., Kelly, S.D., van Nostrand, J., Lowe, K., Mehlhorn, T., Carroll, S., Boonchayanant, B., Loeffler, F., Watson, D., Kemner, D.M., Zhou, J., Kitanidis, P.K., Kostka, J.E., Jardine, P.M., Criddle, C.S., 2010. Effects of nitrate on the stability of uranium in a bioreduced region of the subsurface. Environmental Science and Technology 44, 5104–5111.

Zhang, F., Lui, W., Parker, J.C., Spalding, B.P., Brooks, S.C., Watson, D.B., Jardine, P.M., Gu, B., 2008. Geochemical modeling of reactions and partitioning of trace metals and radionuclides during titration of contaminated acidic sediments. Environmental Science and Technology 42, 8007–8013.

Zhou, Q.Y., Shimada, J., Sato, A., 2001. Three dimensional spatial and temporal monitoring of soil water content using electrical resistivity tomography. Water Resources Research 37, 273–285.